

GSH 23.0–0.7+117, a neutral hydrogen shell in the inner Galaxy

J. M. Stil¹ and A. R. Taylor¹

P. G. Martin^{2,3} and T. A. Rothwell²

J. M. Dickey⁴

N. M. McClure-Griffiths⁵

ABSTRACT

GSH 23.0–0.7+117 is a well-defined neutral hydrogen shell discovered in the VLA Galactic Plane Survey (VGPS). Only the blueshifted side of the shell was detected. The expansion velocity and systemic velocity were determined through the systematic behavior of the H I emission with velocity. The center of the shell is at $(l,b,v)=(23^{\circ}05,-0^{\circ}77,+117 \text{ km s}^{-1})$. The angular radius of the shell is $6'8$, or 15 pc at a distance of 7.8 kpc. The H I mass divided by the volume of the half-shell implies an average density $n_H = 11 \pm 4 \text{ cm}^{-3}$ for the medium in which the shell expanded. The estimated age of GSH 23.0–0.7+117 is 1 Myr, with an upper limit of 2 Myr. The modest expansion energy of 2×10^{48} erg can be provided by the stellar wind of a single O4 to O8 star over the age of the shell. The 3σ upper limit to the 1.4 GHz continuum flux density ($S_{1.4} < 248 \text{ mJy}$) is used to derive an upper limit to the Lyman continuum luminosity generated inside the shell. This upper limit implies a maximum of one O9 star (O8 to O9.5 taking into account the error in the distance) inside the H I shell, unless most of the incident ionizing flux leaks through the H I shell. To allow this, the shell should be fragmented on scales smaller than the beam (2.3 pc). If the stellar wind bubble is not adiabatic, or the bubble has burst (as suggested by the H I channel maps), agreement between the energy and ionization requirements is even less likely. The limit set by the non-detection in the continuum provides a significant challenge for the interpretation of GSH 23.0–0.7+117 as a stellar wind bubble. A similar analysis may be applicable to other Galactic H I shells that have not been detected in the continuum.

¹Department of Physics and Astronomy, University of Calgary, 2500 University Drive N.W., Calgary AB T2N 1N4, Canada

²Department of Astronomy and Astrophysics, University of Toronto, 60 St. George Street Room 1403, Toronto ON, M5S 3H8, Canada

³Canadian Institute for Theoretical Astrophysics, McLennan Labs, University of Toronto, 60 St. George Street, Toronto ON, M5S 3H8, Canada

⁴Department of Astronomy, University of Minnesota, 116 Church Street, SE, Minneapolis, MN 55455, USA

⁵Australia Telescope National Facility, CSIRO, P.O. Box 76, Epping NSW 1710, Australia

Subject headings: ISM: bubbles — ISM: kinematics and dynamics — stars: winds, outflows — ISM: atoms

1. Introduction

The VLA Galactic Plane Survey (VGPS) is part of an international effort to map atomic hydrogen and other tracers of the Galactic interstellar medium with a resolution of $1'$. Previously, large parts of the Galactic plane in the northern sky were covered by the Canadian Galactic Plane Survey (CGPS) (Taylor et al. 2003), and in the southern sky by the Southern Galactic Plane Survey (SGPS) (McClure-Griffiths et al. 2001). The VGPS covers the first Galactic quadrant in the vicinity of the celestial equator, for which the Very Large Array is the most suitable instrument. The VGPS survey area extends from Galactic longitude 18° to 67° . The latitude coverage varies from $|b| < 1^\circ$ at the low longitudes to $|b| < 2^\circ$ at the high longitudes. An outline of the survey area was shown by Taylor et al. (2002).

One important objective of these high resolution H I surveys is to study the effect of stellar wind and supernova explosions on the interstellar medium. There is a rich literature on this subject, and we limit the discussion to some examples that relate to the subject of this paper. The effects of stellar wind and supernovae may be manifested on scales of hundreds of parsecs for super bubbles, chimneys and worms, e.g. Heiles (1979), Heiles (1984), Normandeau et al. (1996), McClure-Griffiths et al. (2000), English et al. (2000), Stil & Irwin (2001), Uyaniker & Kothes (2002), McClure-Griffiths et al. (2002), to ~ 10 pc for winds of single stars. Smaller bubbles originating from a single star may be found around Wolf-Rayet stars (Cappa et al. 2002, for a discussion of radio observations) and some other early type stars, e.g. Higgs et al. (1994), Normandeau et al. (2000), Carral et al. (2002). An interesting question in this respect is what fraction of the stellar wind and supernova ejecta produced in the disk breaks out of the Galactic disk and flows into the Galactic halo. Whether or not a breakout occurs depends on the scale of the bubble and the scale height of H I in the disk. In this context, small bubbles represent events in which matter and energy ejected by massive stars are retained in the disk. As such, smaller bubbles provide a different perspective on the Galactic energy budget, as well as a probe of conditions that relate to the release of enriched matter and energy into the disk and the halo. Parsec scale H I bubbles have become accessible for systematic study through the recent high-resolution H I surveys.

The stellar winds of OB stars are driven by the ultraviolet continuum. Therefore, a strong stellar wind and a high ionizing flux are correlated. A stellar wind bubble can be completely or partly ionized due to the Lyman continuum flux of the central star. It is not clear a priori whether the ionization of a shell can be detected in the radio continuum images of the VGPS. Confusion with unrelated emission may inhibit detection for larger shells. Well-documented examples of smaller shells that would be detectable in a survey such as the VGPS exist in the literature, e.g. Higgs et al. (1994), Cappa et al. (1999). In this paper we present the small H I shell GSH 23.0–0.7+117 discovered in the VGPS, and the implications of its non-detection in the continuum.

2. Observations and data reduction

The data presented in this paper were obtained as part of the VLA Galactic Plane Survey (VGPS). The survey area, observing strategy and data reduction were previously described in Taylor et al. (2002). The VGPS survey area consists of a hexagonal grid of 990 fields observed with the Very Large Array (VLA) D-array, separated by $25'$. Each field was observed as a ~ 3 minute snapshot at 2 to 5 (normally at least 3) different hour angles. In order to obtain sufficient spectral resolution over the velocity range of Galactic H I, the 3-minute observation time for each snapshot was divided into two integrations. In each integration, left and right hand polarization were recorded over a bandwidth of 1.56 MHz in 256 channels (6.1 kHz or 1.28 km s^{-1} per channel), but offset in frequency by 303.06 kHz (49.5 channels). In between integrations, the frequency offset between the polarizations was reversed. The frequency offset provides sufficient line-free channels for continuum subtraction, and complete spectral sampling of the H I line over approximately 240 km s^{-1} . The H I data presented in this paper were sampled with 0.64 km s^{-1} channels.

Information on large-scale structures resolved out by the VLA mosaic was provided by a fast survey of the VGPS area with the Robert C. Byrd Green Bank Telescope (H I line), and the Effelsberg 21-cm survey (Reich & Reich 1986; Reich et al. 1990) for the continuum.

Calibration was carried out using standard procedures within AIPS. The primary calibrators 3C286 and 3C48 were used for flux and bandpass calibration. After calibration, the UV data were imported into MIRIAD for further processing. At the time of submission of this paper, a comparison of continuum source fluxes with the NVSS survey (Condon et al. 1998) indicated that the VGPS flux scale is low by as much as 30% for some fields due to an increase in system temperature by the bright H I line emission. A field-dependent correction based on NVSS source fluxes is currently underway. The flux scale in this paper is based on the calibration of the GBT H I data. One would normally adjust the flux scale of the single dish to the flux scale of the interferometer when the two are combined. Instead, the flux scale of the VLA was divided by 0.85 to match the GBT calibration in the region of the UV plane sampled by both datasets.

Continuum subtraction was done in the UV plane by fitting a linear polynomial to the visibilities in line-free channels. A “dirty” continuum-subtracted mosaic cube, fully sampled on the frequency axis, was then created. The desired $1'$ resolution (FWHM) was obtained by applying an appropriate Gaussian weighting function to the visibilities. A temporary mosaic with (projected) baselines longer than $0.3 \text{ k}\lambda$ was also created, to clean strong compact continuum sources in absorption. These absorbed sources were subtracted from the actual H I images and restored with a Gaussian beam before deconvolution of the line emission. This procedure eliminates the side lobes around absorbed continuum sources, in particular the radial spokes that occur on the 20% level in the dirty beam of VLA snapshots. The H I line emission was then deconvolved with a maximum entropy algorithm (Sault et al. 1996; Cornwell & Evans 1985). The deconvolved model of “clean components” was restored with a $1'$ circular Gaussian beam.

3. Results and analysis

Channel maps of GSH 23.0–0.7+117 are shown in Figure 1. A ring that is open on the lower side is best visible at velocities 113 km s^{-1} to 116 km s^{-1} . At smaller velocities, the radius of this ring decreases until the ring merges into a cap in the velocity range 107 km s^{-1} to 110 km s^{-1} . The systematic behavior of the emission with velocity is characteristic of an expanding H I shell. The principle characteristics that lead to this conclusion are the almost uninterrupted ring morphology and the gradual spatial variation of the line of sight velocity towards the cap in the center. The gradual variation of the velocity towards the center unambiguously associates the cap with the ring, and suggests a line of sight velocity difference of approximately 10 km s^{-1} . It will be shown that this velocity difference implies evolution on a timescale of 1 Myr, which indicates that GSH 23.0–0.7+117 is a transient phenomenon in the interstellar medium.

The circular shape and the regular behavior of the emission as a function of velocity indicate a high degree of symmetry. However, two significant asymmetries are observed. First, virtually no emission of the shell was detected at velocities beyond $\sim 120 \text{ km s}^{-1}$. Instead, the ring-like structure in the channel maps breaks up and fades into the noise at this velocity. Inspection of H I line profiles near the center of the shell shows no evidence for a redshifted cap to the level of the noise. This implies that the blueshifted side of the shell is at least 10 to 20 times brighter than the redshifted side. The H I column density of the blueshifted cap in the center of the shell is $2 \times 10^{20} \text{ cm}^{-2}$. The second asymmetry is that the lower side of GSH 23.0–0.7+117 also appears open. This opening is flanked on both sides by filaments best visible in the channels around 113 km s^{-1} .

The one-sided H I structure could at first sight also be interpreted as a bow shock. The H I brightness in Figure 1 is fairly symmetric relative to the axis $l = 23^\circ 05'$. If H I brightness is primarily a measure of the length of the line of sight through the structure, the line of sight through the top is much longer than through the bottom. This can be the result of a conical geometry, in particular a bow shock due to a moving source with its velocity along the axis of symmetry. To explain the observed brightness distribution, the line of sight through the top of GSH 23.0–0.7+117 should be approximately tangential to the surface of the bow shock. The velocity of the source with respect to the ambient medium would have a component towards the observer (blueshifted cap), and a component towards the Galactic plane. No redshifted side is expected for a bow shock, because the bow shock is open on the far side. However, a bow shock geometry was rejected because of the implied velocity structure. The expansion velocity of a bow shock is locally perpendicular to the surface of the shock. If the line of sight through the top of GSH 23.0–0.7+117 is tangential to the surface of the bow shock, the expansion velocity is perpendicular to the line of sight only at this location. For other lines of sight, the expansion velocity has a line of sight component in the direction of the observer. This implies that the line of sight through the top of GSH 23.0–0.7+117 should dominate the structure in Figure 1 at the most positive velocities. The brightness distribution in Figure 1 does not show the expected concentration of emission towards the top of GSH 23.0–0.7+117 for velocities $v > 115 \text{ km s}^{-1}$.

Since only the approaching side of the shell was detected, a determination of the expansion velocity and the central velocity by visual inspection of the channel maps is not feasible. Following Stil & Irwin (2001), a thin shell model was fitted to the observed line of sight components of the expansion velocity. We fitted Gaussians to the observed line profile at each position to determine the line of sight component of the expansion velocity. On the lower side of the shell the low signal to noise ratio often inhibited a determination of the line of sight velocity. After a number of preliminary fits of the thin shell model, measurements located within 6.6 arcminutes from the center of the shell were included in the analysis.

Models with a systemic velocity less than 117 km s^{-1} resulted in a larger value of χ^2 and were rejected. Models with a systemic velocity larger than 117 km s^{-1} fit the observed line of sight velocities equally well. In this case, the effect of a larger systemic velocity is compensated by a correspondingly larger expansion velocity and a larger radius. This degeneracy is mainly due to the absence of data for the redshifted side of the shell. The degeneracy between the systemic velocity and the expansion velocity was resolved by considering the variation of the radius of the ring of emission in the channel maps with velocity. Figure 2 shows the distance of the peak of the azimuthally averaged brightness profile as a function of velocity. The curves represent restricted thin-shell model fits in which the systemic velocity was fixed to the values indicated in Figure 2. The data are best represented by the curve corresponding with a systemic velocity of 117 km s^{-1} , with an uncertainty of about 1 km s^{-1} . The scatter at smaller radii/velocities is a result of the fact that no clear ring is visible in the corresponding channels. The model with systemic velocity 117 km s^{-1} has an expansion velocity $v_e = 9 \pm 1 \text{ km s}^{-1}$, where the main source of uncertainty is the value of the systemic velocity. The properties of GSH 23.0–0.7+117 are summarized in Table 1.

Figure 3 shows the position-velocity diagram through the center of the shell at constant Galactic latitude. The best-fit model is shown as a white ellipse. Emission at 100 km s^{-1} is clearly identified as a separate velocity component in Figure 3.

The central velocity of GSH 23.0–0.7+117 is close to the extreme positive velocity of Galactic H I at longitude 23° , so the distance is relatively well determined. Assuming a flat rotation curve with $R_0 = 8.5 \text{ kpc}$ and $V_0 = 220 \text{ km s}^{-1}$, the Galactocentric distance is 3.6 kpc , and the heliocentric distance is 6.6 or 9 kpc . This location is close to the extreme end of the Galactic bar (Cole & Weinberg 2002). The assumption of circular orbits in the derived kinematic distance may introduce a significant error. Therefore, we consider the difference between the near and far point not significant and adopt a distance $7.8 \pm 2 \text{ kpc}$. At this distance, the radius of GSH 23.0–0.7+117 is $15 \pm 4 \text{ pc}$, and it is located at $110 \pm 30 \text{ pc}$ below the Galactic plane.

The 21-cm line flux in the velocity range 105 km s^{-1} to 125 km s^{-1} in a circular aperture enclosing the shell is 131 Jy km s^{-1} . Variation of the velocity range by 2 km s^{-1} on each side changes the flux by about 20%, mainly due to a confusing component at 100 km s^{-1} . The H I mass of the shell is then $M_{\text{HI}} = 1.9 \times 10^3 M_\odot$. The total mass of the shell, including 30% helium, is $M_S = 2.5 \times 10^3 M_\odot$. The error in the mass is $\sim 50\%$, dominated by the error in the

distance. The kinetic energy associated with the expansion is $E_{\text{kin}} = 2 \times 10^{48}$ erg, and the expansion momentum (the scalar product of mass and expansion velocity) is $2 \times 10^4 M_{\odot} \text{ km s}^{-1}$. The mass of the shell divided by the volume of the shell provides an estimate of the average density of the medium in which the shell expanded. The resulting density scales only inversely proportional with the assumed distance, and relies further on the plausible assumption that the mass of the shell is dominated by swept-up interstellar gas. The mass of the observed half shell suggests a mean density $n_{\text{H}} = 11 \pm 4 \text{ cm}^{-3}$ when distributed uniformly over the volume of the half-sphere. The error estimate incorporates the effect of uncertainties in the HI line flux, the distance, and the angular radius of the shell, added in quadrature. This density seems quite high, especially for a distance of 110 pc from the Galactic mid plane.

The kinematic age of the shell assuming an expansion law $R \sim t^{0.6}$, appropriate for adiabatic stellar wind bubbles (Weaver et al. 1977), is $t = 0.6R/v_e = 1.0$ Myr. An upper limit to the age of the shell is $t_{\text{max}} = R/v_e = 1.6$ Myr. Taking into account the uncertainties in the distance and the expansion velocity, it is unlikely that the age of the shell is more than 2 Myr.

Figure 4 shows the continuum emission in the vicinity of GSH 23.0–0.7+117. There is no visible counterpart of the H I shell in the continuum image. The faint filamentary structure at longitude 23° extends at least $0^{\circ}.3$ further towards the Galactic equator, and is probably unrelated to GSH 23.0–0.7+117. Figure 5 shows the azimuthally averaged surface brightness in the continuum image as a function of distance from the center of the H I shell. The error bars in Figure 5 (typically 0.24 K) indicate the r.m.s. intensity, divided by the square root of the number of independent beams in each annulus. This is the error in the mean intensity per annulus, taking into account the variance of the background. The error bars do not decrease with radius because the r.m.s. intensity increases with radius due to variation of the background. Figure 5 shows significant excess above the continuum background associated with the H I shell. The 3σ upper limit to the continuum brightness of each annulus above the Galactic background is $T_{\text{b,shell}} < 0.72$ K. The annuli contribute to the flux of the shell with weight proportional to the radius of the annulus. The variance of the weighted sum of the independent annuli is a weighted sum of the variances, where the weights are proportional to the square of the radius of each annulus. The corresponding 3σ upper limit to the flux density of GSH 23.0–0.7+117 in a circular aperture with radius $7'$ is $S_{\nu} < 248$ mJy. The brightness profile of a disk of uniform brightness with this flux density is shown as a dotted line in Figure 5. A stronger upper limit may be found if the continuum emission is assumed to be in a limb-brightened shell similar to the observed H I shell. This would be the case if an ionization front is trapped by the H I shell. Adding the contributions of annuli with radii between $4'$ and $7'$ results in a 3σ upper limit $S_{\nu} < 221$ mJy.

The upper limit to the continuum brightness provides a limit to the emission measure for free-free emission through the relation $\int n_i^2 dl = 562 T_b \text{ cm}^{-6} \text{ pc}$ (for electron temperature $T_e = 7000$ K). For the limb brightened edge of a shell, the length of the line of sight is of the order of the radius of the shell. The upper limit $T_b < 0.72$ K thus implies that the r.m.s. ionized density is bounded by $< n_i^2 >^{0.5} < 5 \text{ cm}^{-3}$. The upper limit $S_{\nu} < 248$ mJy implies the ionized mass is bounded

by $M_i < 1.5 \times 10^3 M_\odot$ (Mezger & Henderson 1967). The upper limit $S_\nu < 221$ mJy for a shell morphology corresponds with $M_i < 1.3 \times 10^3 M_\odot$. These upper limits are smaller than the H I mass of GSH 23.0–0.7+117, which shows that a completely ionized bubble with the same mass as GSH 23.0–0.7+117 would have been detected in the VGPS continuum image.

The foreground extinction was estimated from the total hydrogen column (atomic and molecular at positive velocities) in the direction of GSH 23.0–0.7+117, assuming half of the hydrogen column is in the foreground, $N_H/E(B - V) = 5.8 \times 10^{21} \text{ cm}^{-2} \text{ mag}^{-1}$ (Bohlin et al. 1978), and $A_V/E(B - V) = 3.1$. The resulting foreground extinction is $A_V = 8.6$ magnitudes. As the line of sight to GSH 23.0–0.7+117 is 110 pc from the mid plane at 7.8 kpc, the assumption that half the hydrogen column is in front of GSH 23.0–0.7+117 leads to a probable underestimate of the foreground extinction. No counterpart of GSH 23.0–0.7+117 was found in the VTSS H α survey (Dennison et al. 1999), probably due to the high foreground extinction. Also, no trace of the shell was found in the IRAS 60 μ and 100 μ maps or in the MSX survey (Price et al. 2001). The only entry in the SIMBAD catalog for a position inside the H I shell is the IRAS source IRAS 18332-0907 (l, b)=(23.1, -0.74). The spectrum of this source increases with wavelength, excluding the possibility that it is an obscured star or cluster of stars.

There is no CO emission directly associated with the shell in the survey of Dame et al. (2001). However, a molecular cloud was found at (l, b, v)=(22.78, -1.25, 115.7). The projected distance of this cloud to the center of GSH 23.0–0.7+117 is 68 pc.

4. Discussion

GSH 23.0–0.7+117 is a thin neutral gas shell expanding with a velocity of 9 km s $^{-1}$. Such shells are believed to form when supernovae and or stellar winds interact with the interstellar medium. Although the source is most likely isotropic, the H I morphology of GSH 23.0–0.7+117 is clearly one-sided. It is unlikely that the part of the shell not seen in H I is in fact ionized. If the mass surface density of GSH 23.0–0.7+117 is to be uniform, the mass of the ionized part of the shell must be similar to or more than the H I mass of the neutral part, which is inconsistent with the upper limits to the continuum emission of the shell. It is therefore more likely that the surface density of GSH 23.0–0.7+117 is not uniform. The structure in the channel maps (Figure 1) suggests that the bubble may have burst and that the hot gas interior to the HI shell might flow out of the bubble. The open side of the shell is directed away from the Galactic equator, and away from the observer, suggestive of a density gradient in these directions. The high average density of the ambient medium $n_H = 11 \pm 4 \text{ cm}^{-3}$ found in Section 3 is consistent with the presence of a relatively dense cloud in the vicinity of the source of the shell. A similar front-to-back asymmetry has been observed in other H I shells, e.g. Van der Werf & Higgs (1990), Cappa et al. (1999), Stil & Irwin (2001). A partly ionized shell was not excluded by Van der Werf & Higgs (1990), but a density gradient in the surrounding medium was also suggested by the presence of molecular gas on the side of the H I half shell. Cappa et al. (1999) interpreted the H I filament wrapped around the

Wolf-Rayet ring nebula NGC 2359 as the stellar wind bubble running into a denser cloud on one side. Most of the $\sim 320 M_{\odot}$ neutral mass was reported to be in a hemispherical shell expanding at $6\text{--}7 \text{ km s}^{-1}$.

A first indication of what could be the source of GSH 23.0–0.7+117 is the expansion kinetic energy of 2×10^{48} erg. This amount of energy is readily available in the wind of a single massive star, and only $\sim 0.1\%$ of the kinetic energy released in a single supernova explosion. We shall therefore consider the stellar wind of a single star or a few stars as the energy source of GSH 23.0–0.7+117.

The star(s) inside the shell should be able to provide the expansion energy of the shell. First we determine the average mass loss rate over the age of the shell from the expansion energy. This mass loss rate is then converted into an equivalent number of OB stars. The wind luminosity $L_w = \frac{1}{2} \dot{M} v_w^2$, for a stellar mass loss rate \dot{M} and wind velocity v_w follows from the energy equation

$$\dot{M} v_w^2 t = \frac{M_S v_e^2}{f_w \epsilon_S}, \quad (1)$$

with f_w the fraction of the sphere covered by the H I shell, ϵ_S the efficiency for the conversion of wind kinetic energy into kinetic energy of the shell (Treffers & Chu 1982), t the age of the shell, M_S the mass of the shell and v_e the expansion velocity of the shell. The factor f_w takes into account that the expansion energy of GSH 23.0–0.7+117 incorporates only the incomplete H I shell, whereas the source of the stellar wind is isotropic.

Inspection of the H I channel maps (Figure 1) suggests that $f_w \approx 0.33$. The efficiency $\epsilon_S = 0.2$ for an adiabatic stellar wind bubble was adopted (Weaver et al. 1977). This efficiency may be much lower (Van Buren 1986, for a discussion), but it is unlikely to be much higher. The consequences of $\epsilon_S < 0.2$ will be discussed later in relation to the effect of other model parameters.

The wind velocity of OB stars ranges from 1000 km s^{-1} to 3000 km s^{-1} . Accepting a factor 2 uncertainty in the resulting mass loss rate we assume a wind velocity of 2000 km s^{-1} . The average mass loss rate over the lifetime of the shell is then $\dot{M} = 4 \times 10^{-7} M_{\odot} \text{ yr}^{-1}$. The average mass loss rate was converted into an equivalent number of OB stars with the empirical relation between mass loss rate and luminosity $\log(\dot{M}) = 1.69 \log(L) - 15.4$, with \dot{M} in $M_{\odot} \text{ yr}^{-1}$ and L in L_{\odot} (Howarth & Prinja 1989). The equivalent number of OB stars is the total luminosity derived from this relation, divided by the luminosity of a single star of a specific spectral type. Stellar properties as a function of spectral type were taken from Vacca et al. (1996). This conversion introduces an additional uncertainty of a factor 2 due to the scatter in the empirical relation between mass loss rate and luminosity.

The expansion momentum of the shell provides a consistency check for the mass loss rate derived in this way. The ratio π_S of the momentum of the shell to the momentum carried by the wind over the age of the shell ($\dot{M} v_w t$), is more than 1 for an adiabatic bubble. This is possible because the expansion momentum, the scalar product of the mass of the bubble and its expansion velocity, is increased by the pressure of the hot interior of the bubble. The derived mass loss rate implies that the total wind momentum over the age of GSH 23.0–0.7+117 is $800 M_{\odot} \text{ km s}^{-1}$, so

that $\pi_S = 25$. This ratio is within the range found by Van Buren (1986) for nine stellar wind bubbles.

Figure 6 A shows the equivalent number of OB stars necessary to provide the expansion energy of GSH 23.0–0.7+117 through stellar winds as a function of spectral type. The dashed lines indicate the uncertainty assuming a factor 2 uncertainty in the expansion energy, a factor 2 due to the assumption of a constant wind velocity, and a factor 2 scatter in the empirical relation between luminosity and mass loss rate, added in quadrature. Figure 6 A indicates that the expansion energy of the shell is consistent with (the equivalent of) a single star of spectral type O4 to O8.

If GSH 23.0–0.7+117 is a stellar wind bubble, it can be expected that the star(s) that provided the stellar wind are still present within the shell because the age of the shell is less than the main sequence lifetime of the most massive stars. Although the following discussion is based on the initial assumption that OB stars still exist inside the H I shell, the results that follow can in principle suggest otherwise. The ionizing flux of these stars is bounded by the upper limit of the radio continuum flux derived in Section 3 through the relation (Rubin 1968)

$$f_i L_c = 4.76 \times 10^{39} \nu_{\text{GHz}}^{0.1} d_{\text{pc}}^2 S_{\nu;\text{mJy}} T_e^{-0.45}. \quad (2)$$

Absorption of Lyman continuum photons by dust is neglected. In equation (2) it is assumed that a fraction $(1 - f_i)$ of the Lyman continuum photons escapes from the bubble. This may be because the shell is incomplete, or because the low density part of the shell is fully ionized and does not trap the ionization front. As no evidence for an ionized part of the shell was detected, it can be assumed that $f_i = f_w = 0.33$, provided the observed H I shell intercepts all of the incident ionizing photons. If ionizing radiation leaks through holes in the H I shell not visible at the resolution of the current data, $f_i < 0.33$. Stellar wind bubbles are subject to a number of hydrodynamic instabilities that can cause such fragmentation of the shell (Różyczka & Tenorio-Tagle 1985; García-Segura & Mac Low 1995; García-Segura et al. 1996; Freyer et al. 2003). Inserting $\nu = 1.42$ GHz, $d = 7.8$ kpc, $S_\nu < 248$ mJy, and electron temperature $T_e = 7000$ K, we have $\log(f_i L_c) < 48.5$.

The number of stars of each spectral type that is consistent with the upper limit to the ionizing flux that can be generated inside the H I shell is shown in Figure 6 B-D for three values of f_i . Stellar parameters were taken from Vacca et al. (1996). Note that the solid lines in Figure 6 B-D represent *upper limits* derived from the upper limit to the continuum flux. The dashed lines in Figure 6 B-D indicate the effect of the error in the distance on this upper limit. The shaded areas in Figure 6 B-D indicate the areas where both the energy and the ionization constraints are satisfied, taking into account the uncertainties indicated by the dashed lines. No consistent solution was found for $f_i = 0.33$ (Figure 6 B). This is the case where all the ionizing radiation emitted by the central star(s) in the direction of the observed H I shell is trapped by the shell. Some overlap between the energy and ionization constraints is found for $f_i = 0.1$ (Figure 6 C). In this case, two-thirds of the ionizing flux emitted in the direction of the H I shell by the central star(s) escapes through holes in the H I shell not visible in the present data. In Figure 6 D, 90% of the ionizing radiation escapes in this way. However, this high porosity of the H I shell is less plausible. The detected part of the

H I shell appears continuous in Figure 1. Therefore, a high porosity implies that the shell must be highly fragmented on scales smaller than the beam (2.3 pc).

The size of the region in which both constraints are satisfied, depends also on the model parameters f_w and ϵ_S . The value of f_w is relatively well constrained from the morphology in the H I channel maps. An estimate of the parameter ϵ_S , the ratio of the expansion kinetic energy of the shell to the kinetic energy deposited in the form of stellar wind, involves detailed and in some cases poorly understood physics of the evolution of stellar wind bubbles. However, only an upper boundary to the value of ϵ_S is required here. The value $\epsilon_S = 0.2$ derived by Weaver et al. (1977) for the early stage of evolution (time scale of a few thousand years) provides an adequate limiting value for the purpose of this paper. The conclusions do not change qualitatively unless $\epsilon_S > 0.4$, which is an unlikely high efficiency. A stellar wind bubble in the momentum-conserving phase would have $\epsilon_S \ll 1$. Also, if the bubble did burst, the internal pressure would drop and $\epsilon_S \ll 1$ should be adopted. This eliminates the small overlap between the energy requirement and the ionization constraint in Figure 6, which assumes $\epsilon_S = 0.2$. Therefore, the case $\epsilon_S \ll 1$ creates an even bigger challenge to reconcile the expansion energy of the shell with the limit to the ionizing flux that can be generated inside the shell.

It is concluded from Figure 6 that the equivalent of a single O4 to O8 star is required to provide the expansion energy of GSH 23.0–0.7+117 through a stellar wind. However, the upper limit to the continuum flux of the shell excludes stars with spectral type earlier than O8 unless a significant part of the ionizing flux escapes through holes in the H I shell. A small value of f_i is not implied by the present data, but higher resolution H I observations could verify this. If the bubble burst, as suggested by the morphology in the H I channel maps, or if the bubble is in the momentum conserving phase, the small values of f_i adopted in Figure 6 C and D also fail to provide a solution that satisfies both constraints. It is more likely that a contradiction exists between the spectral type of stars deduced from the dynamics of the shell and the spectral types deduced from the upper limit to the radio continuum flux. In view of this contradiction, the initial assumption that GSH 23.0–0.7+117 is a stellar wind bubble may have to be reconsidered.

If GSH 23.0–0.7+117 is not a stellar wind bubble, its energy source may still be of stellar origin. The H I shell itself provides little or no clue to the nature of its source other than its global properties such as the expansion energy. The shell is as much shaped by the local interstellar medium as it is by its source. We note that the modest expansion energy of GSH 23.0–0.7+117 can be provided by a single star through stellar wind or through a supernova explosion. A supernova explosion would provide the energy without leaving an ionizing source in the shell. One may expect to see a non-thermal radio continuum supernova remnant in this case, although it is not clear whether a radio supernova remnant should still be detectable at the age of GSH 23.0–0.7+117. More sensitive observations of possible ionized gas associated with GSH 23.0–0.7+117, and a similar analysis of other H I shells with or without continuum counterparts can help clarify this issue.

5. Conclusions

We report the discovery of the small H I shell GSH 23.0–0.7+117 in the VLA Galactic Plane Survey (VGPS). The physical parameters of GSH 23.0–0.7+117 are well constrained because its velocity places it close to the tangent point. At $(l, b, v) = (23^{\circ}05, -0^{\circ}77, +117 \text{ km s}^{-1})$, the distance of the shell is $7.8 \pm 2 \text{ kpc}$. The expansion kinetic energy is found to be $2 \times 10^{48} \text{ erg}$ for a shell mass of $2.5 \times 10^3 M_{\odot}$ and expansion velocity $9 \pm 1 \text{ km s}^{-1}$. The age of the shell is 1 Myr with a strong upper limit of 2 Myr. The average density of the medium in which the shell expanded derived from the mass and the volume of the shell is $n_H = 11 \pm 4 \text{ cm}^{-3}$. This relatively high density and the one-sided morphology of the H I shell are suggestive of a density gradient or a cloud in the vicinity of the shell. The H I shell has no counterpart in the VGPS 1.4 GHz continuum image, with an upper limit to the 1.4 GHz flux density $S_{1.4} < 248 \text{ mJy}$.

The interpretation of GSH 23.0–0.7+117 as a stellar wind bubble is tested by combining the energy requirements of the shell with a limit to the number of OB stars inside the shell derived from the upper limit to the 1.4 GHz continuum emission. If GSH 23.0–0.7+117 is an adiabatic stellar wind bubble (Weaver et al. 1977), the expansion energy requires the equivalent of the stellar wind of a single O4 to O8 star. However, the 3σ upper limit to the 1.4 GHz continuum flux density excludes more than one O9 star (O8 to O9.5 given the uncertainty in the distance), unless most of the incident ionizing flux leaks through the H I shell. For this to be the case, the H I shell should be highly fragmented on scales smaller than the beam (2.3 pc). The energy requirements for the shell are significantly larger if the bubble is not adiabatic, or if the bubble has burst, as suggested by the morphology in the H I channel maps. In this case, the discrepancy between the energy requirements of the shell and the maximum number of OB stars allowed inside the shell is even larger.

We conclude that the interpretation of the low-energy H I shell GSH 23.0–0.7+117 as a stellar wind bubble is questionable in view of the absence of continuum emission associated with the shell. A similar argument may be applicable to other Galactic H I shells that have not been detected in the continuum.

6. Acknowledgements

The National Radio Astronomy Observatory is a facility of the National Science Foundation operated under cooperative agreement by Associated Universities, Inc. This research has made use of the SIMBAD database, operated at CDS, Strasbourg, France. The VGPS is supported by a grant to ART from the Natural Sciences and Engineering Council of Canada. We thank the anonymous referee for useful comments about the manuscript.

REFERENCES

- Bohlin, R. C., Savage, & B. D., Drake, J. F. 1978, ApJ, 224, 132
- Cappa, C. E., Goss, W. M., Niemela, V. S., & Ostrov, P. G. 1999, AJ, 118, 948
- Cappa, C. E., Goss, W. M., & Pineault, S. 2002, AJ, 123, 3348
- Carral, P., Kurtz, S. E., Rodríguez. L. F., Menten, K. F., Cantó, G., & Arceo, R. 2002, AJ, 123, 2574
- Cole, A. A., & Weinberg, M. D. 2002, ApJ, 574, L43
- Condon, J. J., Cotton, W. D., Greisen, E. W., Yin, Q. F., Perley, R. A., Taylor, G. B., & Broderick, J. J. 1998, AJ, 115, 1693
- Cornwell, T. J., & Evans, K. F. 1985, A&A, 143, 77
- Dame, T. M., Hartmann, D., & Thaddeus, P. 2001, ApJ547, 792
- Dennison, B., Simonetti, J. H., & Topasna, G. A. 1999 BAAS, 195, 5309
- English, E., Taylor, A. R., Mashchenko, S. Y., Irwin, J. A., Basu, S., & Johnstone, D. 2000, ApJ, 533, L25
- Freyer, T., Hensler, G., & Yorke, H. W. 2003, ApJ, 594, 888
- García-Segura, G., & Mac Low, M.-M. 1995, ApJ, 455, 160
- García-Segura, G., Mac Low, M.-M., & Langer, N. 1996, A&A, 305, 229
- Heiles, C. 1979, ApJ, 229, 533
- Heiles, C. 1984, ApJS, 55, 585
- Higgs, L.A., Wendker, H. J., & Landecker, T. L. 1994, A&A, 291, 295
- Howarth, I. D., & Prinja, R. K. 1989, ApJS, 69, 527
- Mezger, P. G., & Henderson, A. P. 1967, ApJ, 147, 471
- McClure-Griffiths, N. M., Dickey, J. M., Gaensler, B. M., Green, A. J., Haynes, & R. F., Wieringa, M. H. 2000, AJ, 119, 2828
- McClure-Griffiths, N. M., Green, A. J., Dickey, J. M., Gaensler, B. M., Haynes, & R. F., Wieringa, M. H. 2001, ApJ, 551, 394
- McClure-Griffiths, N. M., Dickey, John M., Gaensler, B. M., & Green, A. J. 2002, ApJ, 578, 176
- Normandeau, M., Taylor, A. R., & Dewdney, P. E. 1996, Nature, 380, 687

- Normandeau, M., Taylor, A. R., Dewdney, P. E., & Basu, S. 2000, *AJ*, 119, 2982
- Price, S. D., Egan, M. P., Carey, S. J., Mizuno, D. R., & Kuchar, T. A. 2001, *AJ*, 121, 2819
- Rubin, R. H. 1968, *ApJ*, 154, 391
- Reich, P., & Reich, W. 1986, *A&AS*, 63, 205
- Reich, W., Reich, P., & Fürst 1990, *A&AS*, 83, 539
- Różyczka, M., & Tenorio-Tagle, G. 1985, *A&A*, 147, 202
- Sault, R. J., Staveley-Smith, L., & Brouw, W. N. 1996, *A&AS*, 120, 375
- Stil, J. M., & Irwin, J. A. 2001, *ApJ*, 563, 816
- Taylor, A. R., Stil, J. M., Dickey, J. M., McClure-Griffiths, N. M., Martin, P. G., Rothwell, T. A., & Lockman, F. J. 2002, in *ASP Conf. Ser. 276, Seeing Through The Dust: The Detection Of H I And The Exploration Of The ISM In Galaxies*, ed. A. R. Taylor, T. L. Landecker, & A. G. Wills (San Francisco: ASP), 68
- Taylor, A. R., Gibson, S. J., Peracaula, M., Martin, P. G., Landecker, T. L., Brunt, C. M., Dewdney, P. E., Dougherty, S. M., Gray, A. D., Higgs, L. A., Kerton, C. R., Knee, L. B. G., Kothes, R., Purton, C. R., Uyaniker, B., Wallace, B. J., Willis, A. G., & Durand, D. 2003, *AJ*, 125, 3145
- Treffers, R. R., & Chu, Y.-H. 1982, *ApJ*, 254, 569
- Uyaniker, B., & Kotes, R. 2002, *ApJ*, 574, 805
- Vacca, W. D., Garmany, C. D., & Shull, J. M. 1996, *ApJ*, 460, 914
- Van Buren, D. 1986, *ApJ*, 306, 538
- Van der Werf, P. P., & Higgs L. A. 1990, *A&A*, 235, 407
- Weaver R., McCray R., & Castor, J. 1977, *ApJ*, 218, 377

Table 1. Observed and derived properties of the shell

Quantity	Value
Center longitude	$23^{\circ}050 \pm 0^{\circ}003$
Center latitude	$-0^{\circ}774 \pm 0^{\circ}003$
Systemic velocity	$117 \pm 1 \text{ km s}^{-1}$
Expansion velocity	$9 \pm 1 \text{ km s}^{-1}$
Kinematic distance	$7.8 \pm 2 \text{ kpc}$
Angular radius	$6'.8 \pm 0'.4$
Radius	$15 \pm 4 \text{ pc}$
H I mass	$1.9 \times 10^3 M_{\odot}$
Neutral gas mass	$2.5 \times 10^3 M_{\odot}$
Expansion energy	$2 \times 10^{48} \text{ erg}$
Expansion momentum	$2 \times 10^4 M_{\odot} \text{ km s}^{-1}$
$T_{b,1.4 \text{ GHz}}$	$< 0.72 \text{ K}$
$S_{1.4 \text{ GHz}}$	$< 248 \text{ mJy}$

Fig. 1.— Channel maps of GSH 23.0–0.7+117. The velocities of each channel is indicated in the lower right corner. Brightness temperature is indicated in gray scales linearly from 0 K (white) to 60 K (black). The white contour indicates the 40 K level.

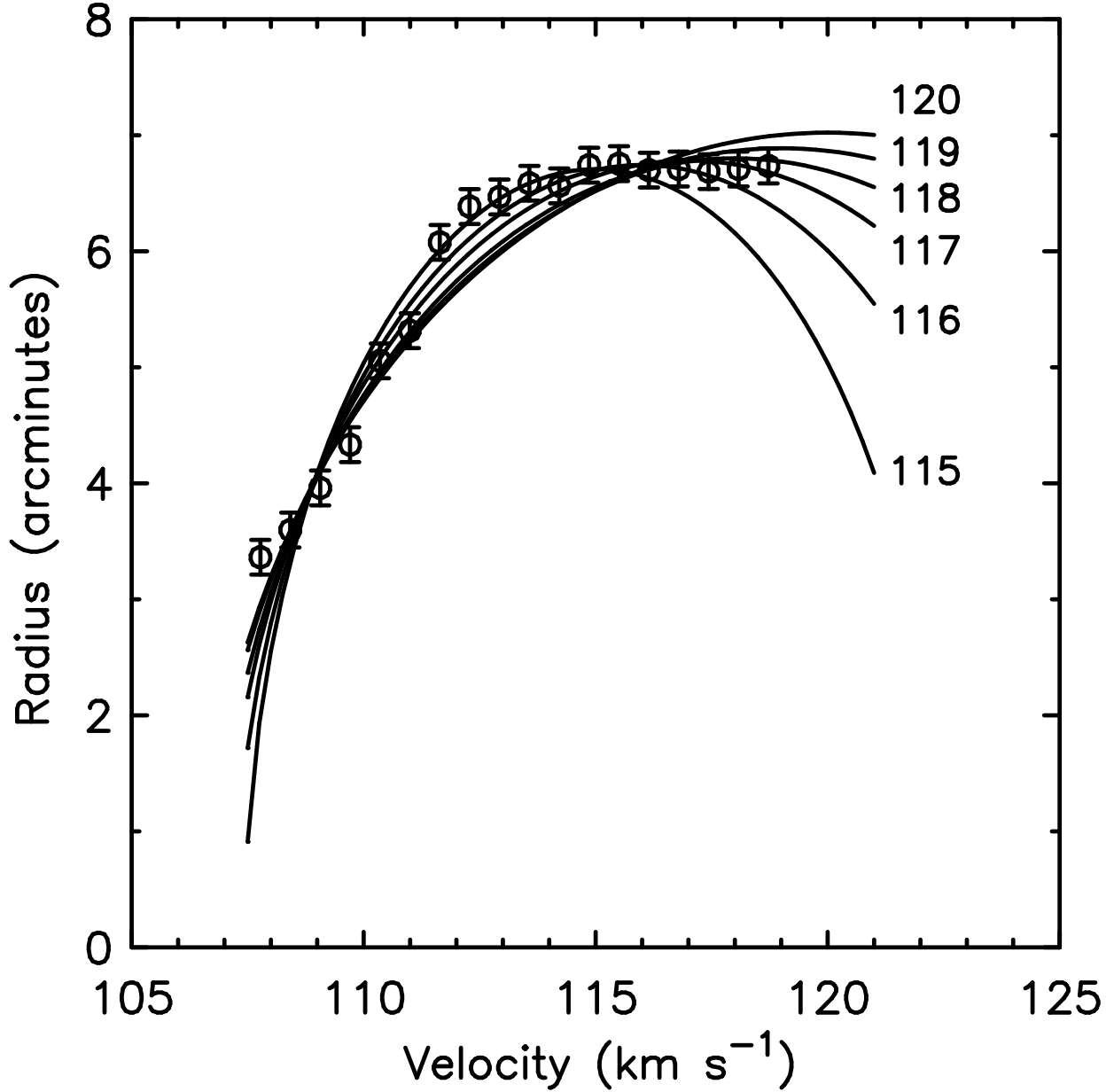


Fig. 2.— Observed radii of the ring of emission associated with the shell as a function of velocity. Error bars indicate the radial bin size used for azimuthal averaging. The curves represent thin expanding shell models that best fit the observed line of sight velocities for a fixed central velocity. The central velocity in km s⁻¹ for each model is indicated.

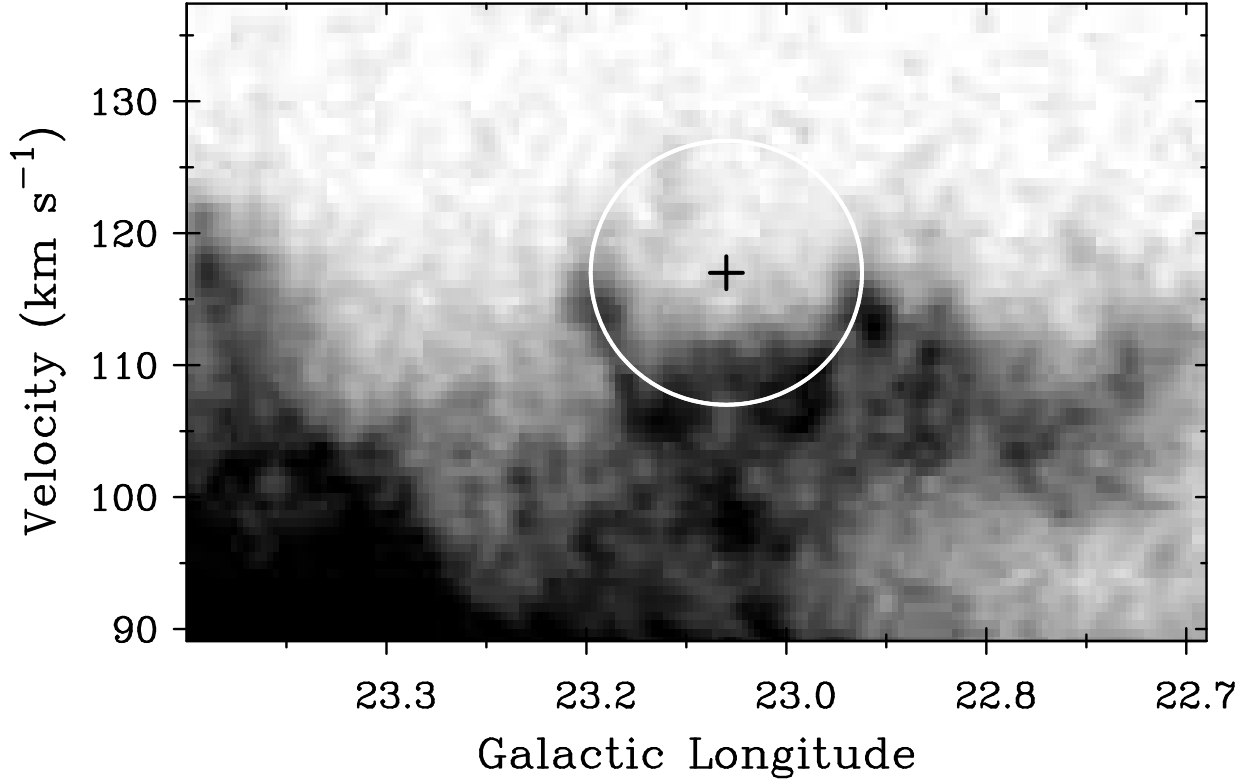


Fig. 3.— Longitude-velocity map through the center of the shell. Brightness temperature is shown as gray scales linearly from 0 K (white) to 50 K (black). The ellipse indicates the best-fit model with parameters listed in Table 1.

Fig. 4.— Continuum emission in the direction of GSH 23.0–0.7+117. Gray scales indicate continuum brightness temperature linearly from 12 K to 40 K. White contours indicate continuum levels from 30 K to 150 K at intervals of 15 K. The black contour shows the outline of GSH 23.0–0.7+117 at the the 22 K level at velocity 114.2 km s⁻¹. The 60'' beamsize is shown in the lower right corner.

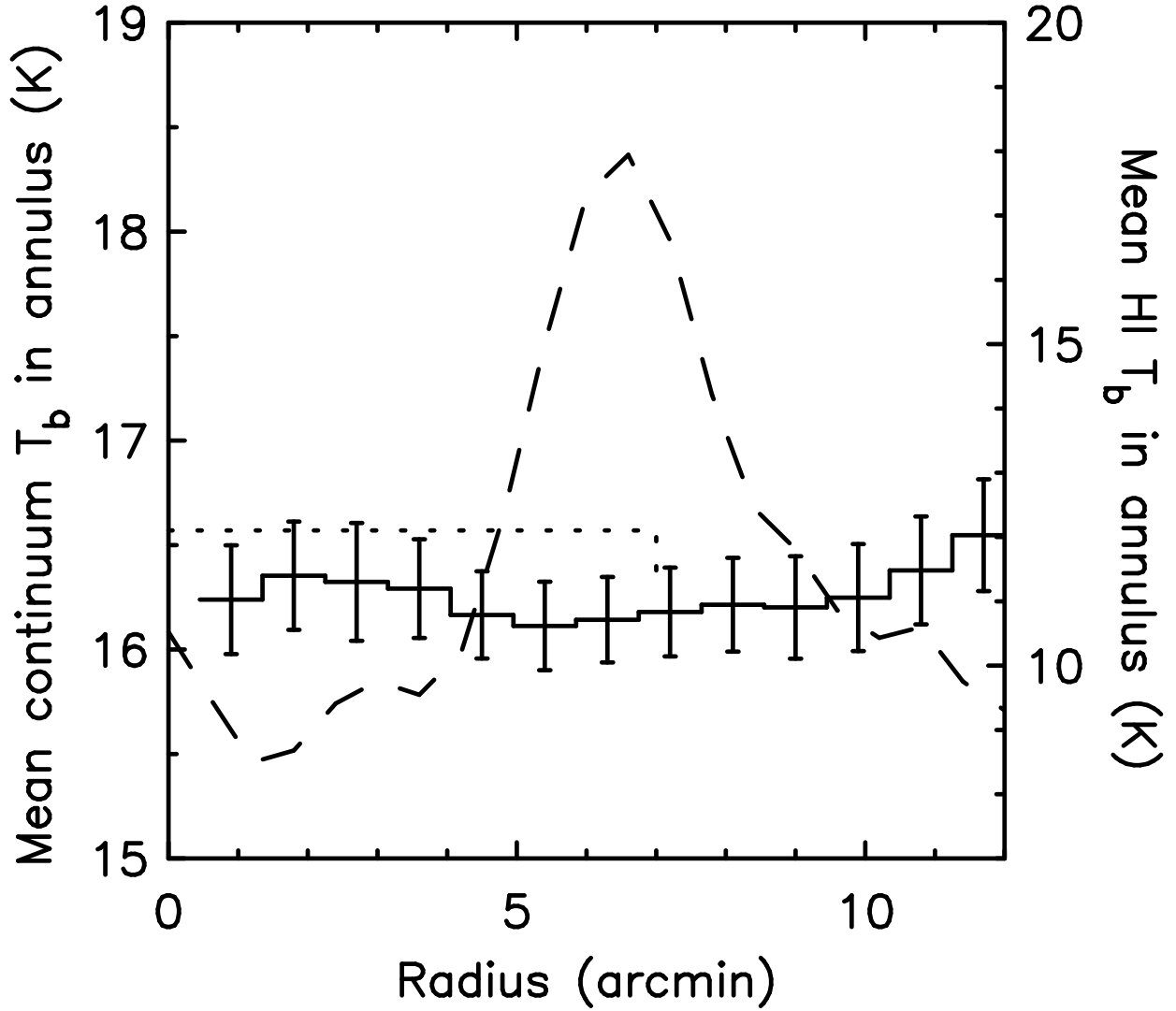


Fig. 5.— Azimuthally averaged surface brightness profile of continuum brightness (histogram; scale on the left axis) and H I at 116.7 km s^{-1} (dashed curve; scale on the right axis). The peak of the dashed line marks the radius of the H I shell. The error bars indicate the error in the mean intensity, defined as the r.m.s. intensity fluctuations divided by the square root of the number of independent beams per annulus. The dotted line shows the surface brightness that corresponds to the 3σ upper limit to the radio continuum flux density $S_\nu < 248 \text{ mJy}$ derived in the text.

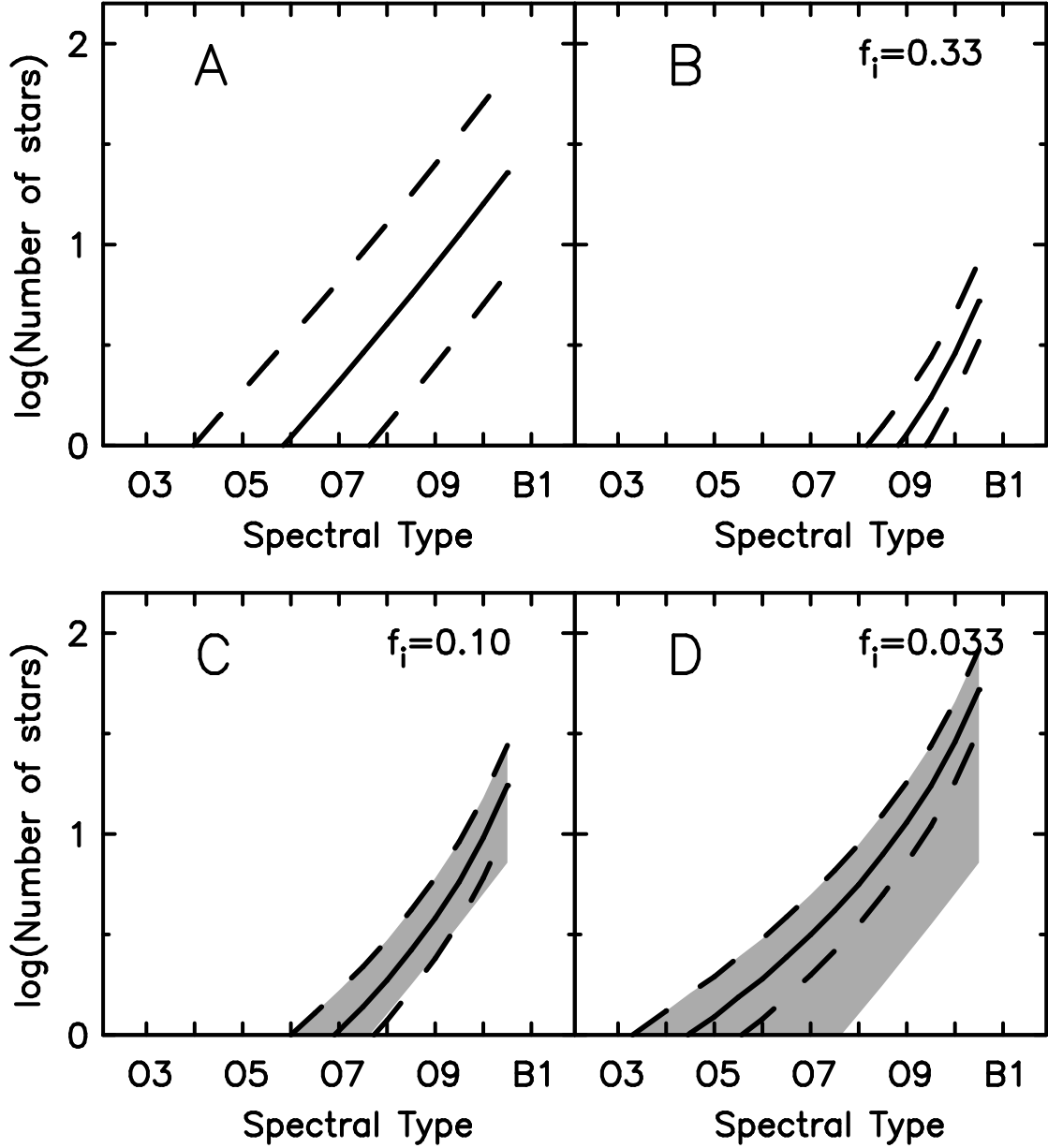


Fig. 6.— A; Number of stars as a function of spectral type that is required to provide the expansion energy of the shell. B: Number of stars inside the shell that is consistent with the upper limit to the continuum for $f_i = 0.33$. C: As B, but for $f_i = 0.1$. D: As B, but for $f_i = 0.033$. The gray shaded areas indicate where the constraints of energy and ionization are both satisfied.

This figure "figure1.gif" is available in "gif" format from:

<http://arxiv.org/ps/astro-ph/0402450v1>

This figure "figure4.gif" is available in "gif" format from:

<http://arxiv.org/ps/astro-ph/0402450v1>